28. Mesleh, M. F., Hunter, J. M., Shvartsburg, A. A., Schatz, G. C. & Jarrold, M. F. Structural information from ion mobility measurements: effects of the long-range potential. *J. Phys. Chem.* **100,** 16082–16086 (1996).
29. Deaven, D. M. & Ho, K. M. Molecular geometry optimization with a genetic algorithm. *Phys. Rev. Lett.* **75,** 288–291 (1995).
30. Jarrold, M. F. Drift tube studies of atomic clusters. *J. Phys. Chem.* **99,** 11–21 (1995).
31. Shvartsburg, A. A., Hudgins, R. R., Dugourd, Ph. & Jarrold, M. F. Structural elucidation of fullerene dimers using high-resolution ion mobility measurements and trajectory calculation simulations. *J. Phys. Chem. A* **101,** 1684–1688 (1997).
32. Bylaska, E. J., Taylor, P. R., Kawai, R. & Weare, J. H. LDA predictions of C_{20} isomerizations: neutral and charged species. *J. Phys. Chem.* **100,** 6966–6972 (1996).
33. Martin, J. M. L. C_{28}: the smallest stable fullerene? *Chem. Phys. Lett.* **255,** 1–6 (1996).

Acknowledgements. We thank J. Chelikowsky, D. Drabold, G. Froudakis, J. Grossman, K. Jackson, K. Jug, M. Krack, U. Landman, H. Mayne, M. Menon, L. Mitas, L. Munro, K. Raghavachari, C. Rohlfing, K. Subbaswamy and D. Wales for providing us with their optimized silicon cluster geometries and for discussions; we also thank R. Hudgins for assistance with the experimental work. This research was supported by the NSF, the US Army Research Office, the Office of Basic Energy Sciences, the High Performance Computing and Communications initiative (including a grant of computer time at the National Energy Research Supercomputing Center), and Ames Laboratory operated for the US DOE by Iowa State University.

Correspondence and requests for materials should be addressed to M.F.J. (e-mail: mfj@chem.nwu.edu).

Interactive effects of ozone depletion and vertical mixing on photosynthesis of Antarctic phytoplankton

Patrick J. Neale*, Richard F. Davis† & John J. Cullen†

* *Smithsonian Environmental Research Center, PO Box 28, Edgewater, Maryland 21037, USA*
† *Center for Environmental Observation Technology and Research, Department of Oceanography, Dalhousie University, Halifax, Nova Scotia B3H 4J1, Canada*

Photosynthesis of Antarctic phytoplankton is inhibited by ambient ultraviolet (UV) radiation during incubations[1–4], and the inhibition is worse in regions beneath the Antarctic ozone 'hole'[4]. But to evaluate such effects, experimental results on, and existing models of, photosynthesis[5–7] cannot be extrapolated directly to the conditions of the open waters of the Antarctic because vertical mixing of phytoplankton alters UV exposure and has significant effects on the integrated inhibition through the water column[2,8,9]. Here we present a model of UV-influenced photosynthesis in the presence of vertical mixing, which we constrain with comprehensive measurements from the Weddell-Scotia Confluence during the austral spring of 1993. Our calculations of photosynthesis integrated through the water column (denoted P_T) show that photosynthesis is strongly inhibited by near-surface UV radiation. This inhibition can be either enhanced or decreased by vertical mixing, depending on the depth of the mixed layer. Predicted inhibition is most severe when mixing is rapid, extending to the lower part of the photic zone. Our analysis reveals that an abrupt 50% reduction in stratospheric ozone could, in the worst case, lower P_T by as much as 8.5%. However, stronger influences on inhibition can come from realistic changes in vertical mixing (maximum effect on P_T of about ±37%), measured differences in the sensitivity of phytoplankton to UV radiation (±46%) and cloudiness (±15%).

When progressively shorter wavelengths of UV are transmitted to samples of phytoplankton, photosynthesis is inhibited in a response that can be described as a function of wavelength[1,2,7,8,10,11]. Results have been used to assess the influence of ozone depletion (which increases the short-wavelength UV-B, 290–320 nm) on primary productivity[2,6,12]. However, simulated vertical mixing of natural samples from the Antarctic showed that inhibition of photosynthesis by UV radiation can be modulated by the temporal pattern of exposure[2]. Because vertical mixing strongly influences open waters of the Antarctic[13,14], models describing inhibition during variable exposure to UV radiation must be developed to quantify the effects of UV and ozone depletion on Antarctic photosynthesis.

An effect of mixing on inhibition is consistent with a response that depends on the history of UV exposure during the day, rather than on instantaneous UV irradiance[15]. Because little is known about the kinetics of inhibition by UV in open waters, we measured the time-course of photosynthesis under combinations of UV radiation and photosynthetically active radiation (PAR; 400–700 nm) for phytoplankton in the Weddell-Scotia Confluence (WSC) and showed that inhibition progressed during exposures to constant irradiance consistent with an exponential survival curve[9], unlike diatoms in culture which quickly reached a stable level of inhibition[15]. Steady-state inhibition in the culture represented a balance between damage and repair processes[15]; in contrast the WSC results implied an absence of repair. Complementary experiments confirmed that recovery processes were insignificantly slow over the timescale of 0.5–3.5 h (ref. 9).

We constructed a model of photosynthesis in mixing surface layers of the WSC to evaluate how this dependence of UV inhibition on cumulative exposure affects P_T. Uninhibited photosynthesis, P_{Tpot}, is calculated for comparison. Previous models using irradiance-dependent inhibition suggested that the effects of ozone depletion

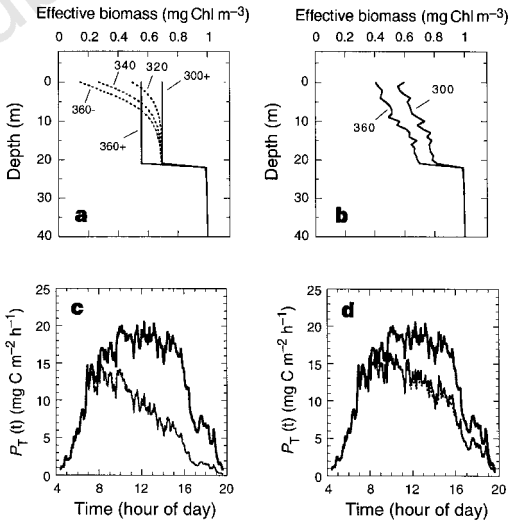

Figure 1 Models of photoinhibition during vertical mixing. **a**, The single-layer model: complete vertical mixing of photosynthetically effective biomass, B_{eff} (mg Chl m^{-3}) to depth z_{mix} is generated at intervals τ_{mix}. During the intervening period, the water is static and B_{eff} declines as a function of cumulative exposure. This example is for $t = 300$ min until 360 min (– and + are before and immediately after 'mixing') on a typical cloudy day (31 October 1993): $z_{mix} = 21$ m, $\tau_{mix} = 1$ h, $O_3 = 300$ DU and B_{eff} initially is 1 mg Chl m^{-3}. B_{eff} for the mixed layer declined to 0.56 from 0.69 mg Chl m^{-3}. The BWF for 3 November was used: on that day, the mixed layer depth was 70 m, so this model predicts the effects of a shoaling in the mixed layer. **b**, A more conventional but computationally intensive lagrangian model of vertical mixing was used to calculate P (equation (1)) for individual particles. Although the distributions with depth seem much more realistic than in the single-layer model, the change in average mixed-layer B_{eff}, to 0.56 from 0.70 mg chl m^{-3} (300–360 min), is almost identical. **c**, The agreement between models extends to the time-course of water-column photosynthetic rate (mg C m^{-2} h^{-1}). The upper curve is uninhibited photosynthesis (irradiance-dependent, hence insensitive to vertical mixing), and the two lower curves (nearly indistinguishable) are the single-layer model (dotted line) and the lagrangian model (solid line). **d**, Water column photosynthetic rate for the single-layer model (lower solid line) compared with the three-layer model (lower dotted line), in which mixing rate decreases with depth (see Methods). This result, for 150 DU, $\tau_{mix} = 1$ h in a 90-m mixed layer, shows that the time course of P_T is insensitive to the assumption of uniform versus decreasing K_z with depth[17], and that P_T is greater for deeper mixed layers.

are small: one model predicted that a 50% depletion would cause a reduction of <1% in P_T for the Southern Ocean south of 50° S[6]; the reduction is <5% in another model for the Bellingshausen Sea[12]. Both models are by definition insensitive to vertical mixing.

Here, we represent inhibition as a decrease in photosynthetically competent biomass (B_{eff}; in units of mg Chl m^{-3}), which in turn decreases photosynthesis (P, in units of mg C m^{-3} h^{-1}; see equation (1) in Methods). At specified time steps, the upper layer (depth ≤ z_{mix}) is 'mixed' by calculating average B_{eff} in the layer, which serves as the initial biomass for the next interval (Fig. 1a). The influence of mixing rate was examined by changing the time step, τ_{mix} (0.16 to 16 h). This idealized representation of vertical mixing over a single layer was validated by comparison to a lagrangian model (Fig. 1b, c; see refs 16, 17) and to a three-layer model in which mixing time increased with depth (Figs 1d and 2b; see refs 17, 18). Using the first model, we examined the influences on P_T of the following; ozone depletion, observed variations in the sensitivity of phytoplankton to UV, depth and rate of vertical mixing, and typical cloudiness versus clear skies.

The analysis revealed complex interactions between UV radiation and vertical mixing. Consistent with experiments using simulated vertical circulation of Antarctic phytoplankton in bottles[2], mixing within the photic zone (z_{mix} ≤ 32 m, depth of 1% surface photosynthetically usable radiation) caused increased inhibition (defined as $1 - (P_T/P_{Tpot})$) as compared to the static case (Fig. 2a, b). A harmful effect of vertical mixing has been suggested previously on the basis of experimental results on Antarctic phytoplankton[2,19], but mechanistic explanations could not be developed from available information. Here, the negative effect of mixing is the consequence

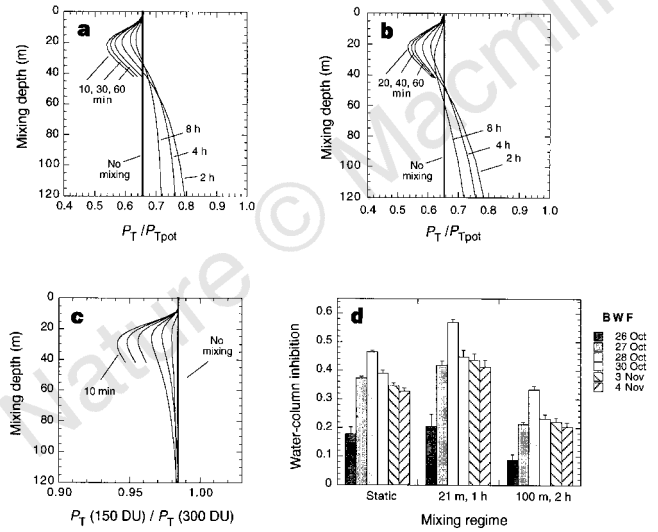

Figure 2 Model results constrained by direct measurements from the WSC[9]. **a**, Interactive effects of mixing depth and mixing timescale (curves labelled with τ_{mix}) on daily water-column productivity relative to the uninhibited rate, using the biological weighting function (BWF) of 3 November 1993, O_3 = 300 DU. Langmuir circulation can mix the upper water column rapidly, so mixing times ≤1 h are modelled for mixing depths ≤42 m. **b**, As in **a**, except for the three-layer mixing model (Fig. 1d). Nominal times are τ_{mix} for the upper two layers. **c**, Interactive effects of O_3 depletion (150 DU versus 300 DU) and mixing time as a function of mixing depth: proportional change in P_T for the same curves as in **a**. **d**, Water-column inhibition defined as $(1 - (P_T/P_{Tpot})$; 300 DU) evaluated with the six BWFs from the WSC under three different conditions: no mixing, mixing to 21 m (τ_{mix} = 1 h), and mixing to 100 m (τ_{mix} = 2 h). Range bars indicate the enhancement of inhibition (relative to P_{Tpot} for 300 DU) associated with 50% O_3 depletion. The no-mixing example approximates results for day-long fixed-depth incubations[4]; results for shallow mixing are more relevant for the first three BWFs (sampled from mixed layers of about 30, 35 and 25 m); and the results for deep mixing better represent the latter three BWFs (from mixed layers of about 100, 70 and 120 m).

of the exponential decline of photosynthetic competence as a function of cumulative exposure (H^*_{inh}, dimensionless; see equation (1b) in Methods). For severe near-surface inhibition in the static case (H^*_{inh} = 4 for exposure symmetrical about midday), inhibition ($1 - (P/P_{pot})$; see ref. 9) is 0.76 for the full day, as observed for some incubations in containers[19,20]. However, 75% of the inhibition (0.57/0.76) occurs during the first half of the day. In the afternoon under these static conditions, surface phytoplankton are already strongly inhibited, so decrements of B_{eff}, hence P, are smaller. Vertical mixing brings deeper, less inhibited phytoplankton to the surface and more photosynthetic biomass is inactivated through the day. Also, inhibited phytoplankton are transported to the lower photic zone where light-limited rates are reduced as compared to the static case. Consequently, P_T is lower when the water is mixed within the photic zone. The process is analogous to models of the destruction of pollutants[21] or viruses[22] by UV radiation because, for the phytoplankton we studied, inhibition is a function of cumulative exposure, essentially irreversible for the timescale we consider (<1 d).

In contrast, mixing well below the photic zone lessens inhibition (Fig. 2a). In the model, deep vertical mixing maintains high B_{eff} at the surface, hence high rates of inactivation ($\Delta B_{eff}/\Delta t$). Although reductions of integrated B_{eff} (mg Chl m^{-2}) are greatest for deep vertical mixing, the damage is distributed over a greater depth, so changes in B_{eff} (mg Chl m^{-3}) within the photic zone are small (compare ref. 8). Simply, deep mixing has a net positive effect on P_T because deep phytoplankton represent a large reservoir of photosynthetic competence that would not contribute to P_T if it were not for vertical mixing. This compensation effect is less pronounced when mixing time increases with depth (Fig. 2b) so that residence time below the photic zone is longer. In the extreme, slow mixing is equivalent to no mixing, so both the negative and positive influences of vertical mixing are stronger for shorter mixing timescales in the model (Fig. 2a, b).

The depth and rate of vertical mixing influence not only overall inhibition, but also the incremental effects of changes in stratospheric ozone. For one example (Fig. 2c), predicted P_T for static water under severe O_3 depletion (150 Dobson units, DU) was 1.5% lower than under more normal 300 DU. Incremental inhibition (defined as $1 - P_T(150\,DU)/P_T(300\,DU)$) was maximal (5.9%) for rapid mixing to 30 m, and was less for shallower, deeper or slower mixing.

Measured sensitivity to UV radiation, quantified by biological weighting functions (BWFs; see equation (2) in Methods), varied by more than a factor of three between phytoplankton assemblages in the WSC[9], strongly affecting water-column inhibition. For an example presented here (Fig. 2d), differences in sensitivity to UV were responsible for about a threefold range in modelled inhibition, regardless of mixing regime. This large variation demonstrates that one BWF cannot describe responses of Antarctic phytoplankton to UV[6,7], even if the spectral slopes of BWFs are similar[10]. Physiological variability also altered the interaction between vertical mixing and O_3 depletion, although subtly. Incremental inhibition associated with 50% O_3 depletion (range bars in Fig. 2d) was generally small (<10%), but higher for the assemblages that were less sensitive to UV. This is in part a consequence of the nonlinear dependence of inhibition on cumulative exposure (equation (1b) in Methods): effects of incremental H^*_{inh} are less when H^*_{inh} is already large.

A sensitivity analysis, constrained by direct measurements in the WSC, allows us to compare the relative influences of O_3 depletion, physiological variability, hydrographical variability and cloudiness on primary productivity in open waters of the Antarctic (Table 1). The range of modelled conditions is generally consistent with what we encountered in the WSC, with the exception of mixed layers <20 m and the extremes of O_3 concentration. Results indicate that O_3 depletion has a consistently negative effect on primary production during the spring. For the worst combination of BWF, mixing depth and mixing time, P_T was reduced by 6.2% (cloudy) to 8.5%

(clear sky) by 50% O_3 depletion, approximately the greatest depletion encountered during the cruise. For most modelled conditions, however, the reduction of P_T was a few per cent in response to 50% O_3 depletion. Measured variability in the sensitivity of phytoplankton to UV radiation (that is, BWFs) had a much greater influence; it is responsible for a range of as much as ±46% (more commonly near ±25%) in P_T under a particular regime of irradiance and mixing. Similar strong influences on P_T are associated with vertical mixing. Although there is an interaction between mixing rate and mixing depth (Fig. 2), the extreme positive and negative effects (+31% and −44%) of mixing are associated with deep and shallow mixing, respectively, at the shortest mixing times. The influence of vertical mixing is less for longer mixing times (Fig. 2a) and for other combinations of BWF and O_3 depletion, yet generally greater than the effects of O_3 depletion. Typical cloudy conditions, as compared to clear skies, had a variable, though mostly negative influence on P_T. Decreased PAR would reduce P_{Tpot} by 24–27%; however, inhibition also decreases under cloudy skies, so the net effect of clouds on P_T ranged from −24% to +5.7%, depending on vertical mixing and the sensitivity of phytoplankton to UV.

Our analysis differs in several respects from previous attempts to quantify photoinhibition in Antarctic phytoplankton: (1) BWFs were determined on the same assemblages for which P_T is modelled; (2) the dependence of photoinhibition on irradiance was explicitly rejected through experimentation and an appropriate model was developed; (3) the effects of vertical mixing (mixing rate and mixing depth) on P_T are quantified; and (4) results for typical cloudy conditions are compared with those for a clear sky. Still, two fundamental results of the analysis were consistent with previous findings[2,4,12]: inhibition of P_T by UV radiation under normal O_3 conditions was very significant (often >20%), and O_3 depletion made it worse, although only by a few per cent. Because estimates of UV effects on Antarctic phytoplankton are generally based in one way or another on fixed-depth incubations, it is encouraging that our results for static conditions compare well to what has been published: simulations of vertical mixing (Fig. 2) illustrate how fixed-depth incubations can yield biased results (see also ref. 2).

We are confident that the results of our analysis describe the fundamental relationships between vertical mixing, solar radiation, and physiological responses of WSC phytoplankton to UV radiation, yet our results must be treated with great caution. First, it should be recognized that for each BWF, inhibition by UV can be accurately assessed only for the set of conditions on the day of sampling. The sensitivity analysis predicts what would happen if mixing, cloudiness or O_3 changed abruptly. For example, if a sensitive assemblage from a deep mixed layer or an uplifted stratum is trapped in a shallow mixed layer (as seems to have occurred on 28 October during the WSC cruise; ref. 9), severe inhibition should ensue (Fig. 2d). By the next day, acclimatization[23] as well as differential survival is likely to engender an assemblage more tolerant to UV, like those sampled from relatively shallow mixed layers[9]. Thus the largest inhibitions in our sensitivity analysis would represent possibly rare, transient events.

It should also be remembered that our model of inhibition (equation (1)), dependent on cumulative exposure and irreversible, was developed on the basis of short-term (0.5–3.5 h) experiments on phytoplankton from cold, deeply mixed surface layers[9]. It is possible that the feeble ability to repair damage to photosynthetic systems is the consequence of very low rates of respiration and growth in these light-limited phytoplankton (see ref. 14). If recovery could proceed on timescales of several hours to a day, some patterns in our data would be tempered, but not eliminated. We know that short-term irreversibility of inhibition does not hold for temperate phytoplankton in culture[15] or for Antarctic phytoplankton from more protected waters[7] where mean irradiance is probably higher and where repair mechanisms may be more active. Clearly, models should be modified as more information on the kinetics of inhibition and recovery in Antarctic waters becomes available.

Although the average effects in Table 1 reflect somewhat the choices that were made for inclusion in the sensitivity analysis, the ranges represent natural variability in Antarctic waters. We conclude that ozone depletion can inhibit primary productivity in open

Table 1 Influences on water-column productivity

		Per cent change					
		Strongest effect		Weakest effect		Average	
		Cloud	Clear	Cloud	Clear	Cloud	Clear
Source of variability	Measure of variability						
Ozone depletion*	$\frac{P_T(150\,DU) - P_T(300\,DU)}{P_T(300\,DU)}$	−6.2	−8.5	−0.8	−0.7	−2.7	−2.8
Physiological variability†	$P_T/(P_{Tpot}(300\,DU))$	±36.1	±45.5	±13.9	±17.3	±24.5	±28.0
Depth of vertical mixing	$\frac{P_T(z_{mix}) - P_T(static)}{P_T(static)}$	−32.2 +30.9	−43.8 +29.7			−16.5 +24.8	−27.3 +21.4
Effect of cloudiness on inhibition§	$(P_T/P_{Tpot})[cloud] - (P_T/P_{Tpot})[clear]$	+14.3		+0.7		+6.2	
Effect of cloudiness on P_{Tpot}	$\frac{P_{Tpot}(cloud) - P_{Tpot}(clear)}{P_{Tpot}(clear)}$	−26.7		−23.5		−24.9	
Net effect of cloudiness	$\frac{P_T(cloud) - P_T(clear)}{P_T(clear)}$	−24.3‖		+5.7¶		−16.1	

Data are the results of a sensitivity analysis using a model of water-column productivity constrained by direct measurements in the Weddell–Scotia Confluence. Per cent changes are presented for a typical cloudy day (31 October 1993) and for clear skies. Averages are very rough measures of central tendency, because they are influenced by the choice of conditions for the sensitivity analysis.

* The potential effect of an abrupt, 50% reduction in stratospheric ozone (see ref. 4) is represented as the per cent reduction of P_T (mg C m^{-2} d^{-1}) for 150 DU as compared to 300 DU. The strongest and weakest effects are the extremes for all combination of conditions (6 BWFs, 21 z_{mix} and 10 τ_{mix}). Mixing times ≤1 h are not considered for z_{mix} > 42 m.

† Effects of physiological variability are quantified as the range of $P_T/(P_{Tpot}(300\,DU))$ for the six measured BWFs, normalized to the mean value for the six, evaluated for each combination of nine O_3 concentrations, 21 z_{mix} and 10 τ_{mix}. Results are expressed as ± half this range. Productivity was normalized to P_{Tpot} to focus on variability associated with differences in sensitivity to UV. P_{Tpot} is evaluated at 300 DU so that variations in the small increase of P_{Tpot} associated with O_3 depletion[6] are considered.

‡ Extreme per cent reductions or enhancements associated with mixing for all combinations of BWF, z_{mix} and O_3. As z_{mix} and τ_{mix} are varied (Fig. 2a) the reduction of P_T is always greatest for the most rapid mixing (τ_{mix} = 10 min) to an intermediate depth and maximum enhancement is for the most rapid, deepest mixing (τ_{mix} = 1.5 h, z_{mix} = 120 m). The average effects of mixing depth are reported as means of the maximum reductions and enhancements for the 54 combinations of BWF and O_3 concentration. Effects approach zero as mixing rate slows.

§ Effects of cloudy conditions as compared to clear skies for all combinations of O_3, BWF, z_{mix} and τ_{mix}. The combinations of conditions associated with the strongest and weakest reductions of inhibition are not the same as those for the strongest and weakest reductions of P_{Tpot}.

‖ The greatest reduction of P_T associated with cloudiness.

¶ The greatest enhancement of P_T associated with cloudiness.

waters of the Antarctic, but that natural variability in exposures of phytoplankton to UV radiation, associated with vertical mixing and cloud cover, has an important role in either enhancing or diminishing the effect on water-column photosynthesis. Vertical mixing and UV radiation interact both directly in their effects on photosynthesis, and indirectly by influencing acclimatization and selection of phytoplankton. It should be recognized, however, that regardless of these natural interactions, UV radiation presents a significant environmental stress, and its effects are enhanced by ozone depletion. □

Methods

Calculation of water-column photosynthesis. The bio-optical model of Arrigo[6], which incorporated our laboratory-derived model of PAR-dependent photosynthesis as inhibited by UV radiation[11], was modified to include our field-based biological model and time courses of UV and PAR exposure for given rates and depths of vertical mixing as represented by three alternative physical models.

Biological model. Photosynthesis, P (mg C m^{-3} h^{-1}), is a saturating function of the irradiance absorbed by photosynthetic systems (photosynthetically usable radiation[24], E_{PUR}, μmol m^{-2} s^{-1}), relative to a saturating value, E_k (μmol m^{-2} s^{-1}):

$$P = P_s^{B_{eff}}(1 - e^{-E_{PUR}/E_k})B_{eff} \quad (1a)$$

$$B_{eff}(T) = B_{eff}(0)e^{-H^*_{inh}} \quad (1b)$$

P is constrained by $P^{B_{eff}}{}_s$ (mg C (mg Chl)$^{-1}$ h^{-1}), the maximum potential rate normalized to photosynthetically effective chlorophyll biomass, B_{eff} (mg Chl m^{-3}). Inhibition is represented as exponential inactivation of B_{eff} as a function of biologically effective exposure, H^*_{inh} (dimensionless). This definition simplifies the calculation of inhibition during mixing; we are not assuming destruction of pigment. H^*_{inh} is evaluated using a biological weighting function (BWF)[25], a set of weightings ($\epsilon_H(\lambda)$, reciprocal μmol m^{-2}) that quantify effectiveness of spectral exposure ($E(\lambda)$, μmol m^{-2} s^{-1} nm^{-1}, integrated over time, T) as a function of wavelength:

$$H^*_{inh} = \int_0^T \left(\sum_{\lambda=280\,nm}^{700\,nm} \epsilon_H(\lambda)E(\lambda)\Delta\lambda \right) dt \quad (2)$$

Uninhibited photosynthesis, P_{pot}, is calculated by setting $H^*_{inh} = 0$. Photosynthetic parameters in equation (1) and BWFs for equation (2) were experimentally determined on six occasions during October and November 1993[9].

Physical model: single-layer mixing.

Step a.

$$\left\{ \begin{matrix} E_{dd}(\lambda, 0^+, t) \\ E_{ds}(\lambda, 0^+, t) \end{matrix} \right\} \xrightarrow{\rho, \rho', \bar{\mu}_d} E(\lambda, 0^-, t) \xrightarrow{K(\lambda)} E(\lambda, z, t)$$

Step b.

$$E(\lambda, z, t) \xrightarrow{\bar{a}_{ps}(\lambda)} E_{PUR}(z, t)$$

$$E(\lambda, z, t) \xrightarrow{\epsilon_H(\lambda)} H^*_{inh}(z, t)$$

Step c.

$$B_{eff}(t = 0) \xrightarrow{H^*_{inh}(z,t)} B_{eff}(z, t) \qquad [z_{mix} \leqslant z \leqslant 120\,m]$$

$$B_{eff}(t = 0) \xrightarrow{H^*_{inh}(z, t), \tau_{mix}, f(z_{mix})} B_{eff}(z, t) \qquad [0 \leqslant z \leqslant z_{mix}]$$

Step d.

$$P_T = \sum_{z=0}^{120\,m} \sum_{t=0}^{16\,h} P(E_{PUR}(z, t), B_{eff}(z, t))\Delta t \Delta z$$

Step a, A clear-sky solar radiation model[26], with enhanced spectral resolution in the UV[6] is used to calculate the direct (E_{dd}) and diffuse (E_{ds}) components of downwelling spectral irradiance just above the surface ($E(\lambda,0^+,t)$; μmol m^{-2} s^{-1} nm^{-1}), consistent with local meteorology (59.6° S, 52.1° W, 31 October 1993); column O_3 is varied in a sensitivity analysis. Attenuation by clouds, from the ratio of shipboard pyranometer readings to clear-sky predictions (cloud index, CI) for this typical cloudy day, is considered to be spectrally neutral[12]; the resulting increase of E_{ds} as the expense of E_{dd} is calculated from an empirical relationship between CI and direct versus global shortwave irradiance[27] for each model time-step (Δt) of 5 min. Spectral scalar irradiance just below the surface, $E(\lambda,0^-,t)$, is obtained by accounting for surface reflection of E_{dd} and E_{ds} (ρ and ρ'), refraction, and the contribution of direct and diffuse components to $\bar{\mu}_d$, the average cosine of the downwelling radiance distribution[28]; upwelling irradiance was ignored. A profile of downwelling irradiance in four UV-wavebands (PUV-510, Biospherical Instruments) was used to estimate diffuse attenuation coefficients ($K(\lambda)$, m^{-1}), from 290 to 380 nm, with linear interpolation and extrapolation of $K(\lambda)$ versus λ. Estimates of spectral attenuation in the visible (LiCor submersible spectroradiometer) were merged to estimate $K(\lambda)$ from 290 to 700 nm, and $E(\lambda,z,t)$ was estimated as $E(\lambda,0^-,t)\exp(-K(\lambda)\cdot z)$. **Step b**, $E(\lambda,z,t)$ is weighted by a normalized fluorescence excitation spectrum, $\bar{a}_{ps}(\lambda)$, for a diatom[29] to calculate $E_{PUR}(z,t)$ (ref. 24) for equation (1a); $H^*_{inh}(z,t)$ comes from equation (2), using $E(\lambda,z,t)$ and directly measured BWFs, $\epsilon_H(\lambda)$, for WSC phytoplankton[9]. **Step c**, Effective biomass, $B_{eff}(z,t)$, is evaluated for each time step (equation (1b)) using BWF results (equation (2)). At dawn ($t = 0$), B_{eff} is constant with depth, consistent with measurements on discrete samples within mixed layers in the study region. For stratified water ($z_{mix} \leqslant z \leqslant 120$ m), $B_{eff}(z,t)$ depends only on H^*_{inh} at depth z from dawn through time t. Under the influence of mixing ($0 \leqslant z \leqslant z_{mix}$), water is static for the mixing period, τ_{mix} (h); before the next time-step, $B_{eff}(z)$ is instantaneously and evenly redistributed in the mixed layer, retaining the same average concentration (Fig. 1a). **Step d**, Photosynthesis, $P(z,t)$ (mg C m^{-3} h^{-1}) is calculated from $E_{PUR}(z,t)$ and $B_{eff}(z,t)$ using $P^{B_{eff}}{}_s$ and E_k from the same BWF experiments (equation (1a)). Daily photosynthesis integrated through the water column, P_T (mg C m^{-2} d^{-1}), is calculated by numerical integration through time and over depth, and uninhibited P_{Tpot} ($H^*_{inh} = 0$) is calculated for reference.

Lagrangian mixing model. Irradiance was specified using steps a and b, above. Then lagrangian trajectories were specified for 2,000 particles during simulated mixing from winds of 10 m s^{-1} (ref. 16, after ref. 17) corresponding to a timescale for vertical movement (z_{mix}/(modelled turbulent r.m.s. velocity))[30] of ~0.6 h for a mixed layer of 21 m. $E(\lambda,z,t)$ along the trajectory was used to evaluate P (equation (1)) for each particle. Because changes of mixing rate with depth in the mixed layer cannot be characterized robustly for this region, the coefficient of eddy diffusion K_z was assumed to be constant through the mixed layer, instead of declining with depth as in the original model[17].

Three-layer mixing. To simulate decreased mixing with depth in the surface layer (see ref. 18), mixing is like the single-layer model, except that the mixed layer is divided in three and mixing occurs at intervals of 0.5 τ_{mix} in the upper third of the mixed layer, τ_{mix} for the upper two layers, and 2.0 τ_{mix} for all three layers.

Sensitivity analysis. The analysis was run using the single-layer model: for each of six sets of BWF parameters determined on phytoplankton from the WSC; under both cloudy and clear-sky conditions; varying z_{mix} from 0 to 120 m ($N = 21$); τ_{mix} from 0.16 to 16 h ($N = 10$); and O_3 from 75 to 450 DU ($N = 9$). A less comprehensive analysis was run with the three-layer model, yielding similar results. Mixing rates were not measured in the rough, windy WSC during our study (mean wind speed, 14.6 m s^{-1}; mixed layer depths, 25–120 m during the October–November 1993 cruise), so we modelled a range of timescales that probably encompass conditions in open waters of the Antarctic[13,30]. Mixing times ⩽1 h are not considered for $z_{mix} > 42$ m.

Received 29 July 1997; accepted 10 February 1998.

1. Lubin, D. *et al.* A contribution toward understanding the biospherical significance of Antarctic ozone depletion. *J. Geophys. Res.* **97,** 7817–7828 (1992).
2. Helbling, E. W., Villafañe, V. & Holm-Hansen, O. in *Ultraviolet Radiation in Antarctica: Measurements and Biological Effects* (eds Weiler, C. S. & Penhale, P. A.) 207–227 (Am. Geophys. Union, Washington DC, 1994).
3. Vernet, M., Brody, E. A., Holm-Hansen, O. & Mitchell, B. G. in *Ultraviolet Radiation in Antarctica: Measurements and Biological Effects* (eds Weiler, C. S. & Penhale, P. A.) 143–158 (Am. Geophys. Union, Washington DC, 1994).
4. Smith, R. C. *et al.* Ozone depletion: Ultraviolet radiation and phytoplankton biology in Antarctic waters. *Science* **255,** 952–959 (1992).
5. Neale, P. J., Lesser, M. P. & Cullen, J. J. in *Ultraviolet Radiation in Antarctica: Measurements and Biological Effects* (eds Weiler, C. S. & Penhale, P. A.) 125–142 (Am. Geophys. Union, Washington DC, 1994).
6. Arrigo, K. R. Impact of ozone depletion on phytoplankton growth in the Southern Ocean: large-scale spatial and temporal variability. *Mar. Ecol. Prog. Ser.* **114,** 1–12 (1994).
7. Boucher, N. & Prézelin, B. B. An *in situ* biological weighting function for UV inhibition of phytoplankton carbon fixation in the Southern Ocean. *Mar. Ecol. Prog. Ser.* **144,** 223–236 (1996).

8. Smith, R. C. & Baker, K. S. in *The Role of Solar Ultraviolet Radiation in Marine Ecosystems* (ed. Calkins, J.) 509–537 (Plenum, New York, 1982).
9. Neale, P. J., Cullen, J. J. & Davis, R. F. Inhibition of marine photosynthesis by ultraviolet radiation: Variable sensitivity of phytoplankton in the Weddell-Scotia Confluence during the austral spring. *Limnol. Oceanogr.* (in the press).
10. Behrenfeld, M. J., Chapman, J. W., Hardy, J. T. & Lee, H. II Is there a common response to ultraviolet-b radiation by marine phytoplankton. *Mar. Ecol. Prog. Ser.* **102,** 59–68 (1993).
11. Cullen, J. J., Neale, P. J. & Lesser, M. P. Biological weighting function for the inhibition of phytoplankton photosynthesis by ultraviolet radiation. *Science* **258,** 646–650 (1992).
12. Boucher, N. P. & Prézelin, B. B. Spectral modeling of UV inhibition of *in situ* Antarctic primary production using a field derived biological weighting function. *Photochem. Photobiol.* **64,** 407–418 (1996).
13. Veth, C. The evolution of the upper water layer in the marginal ice zone, austral spring 1988, Scotia-Weddell Sea. *J. Mar. Syst.* **2,** 451–464 (1991).
14. Nelson, D. M. & Smith, W. O. Jr Sverdrup revisited: Critical depths, maximum chlorophyll levels, and the control of Southern Ocean productivity by the irradiance-mixing regime. *Limnol. Oceanogr.* **36,** 1650–1661 (1991).
15. Cullen, J. J. & Lesser, M. P. Inhibition of photosynthesis by ultraviolet radiation as a function of dose and dosage rate: Results for a marine diatom. *Mar. Biol.* **111,** 183–190 (1991).
16. Franks, P. J. S. & Marra, J. A simple new formulation for phytoplankton photoresponse and an application in a wind-driven mixed-layer model. *Mar. Ecol. Prog. Ser.* **111,** 145–153 (1994).
17. Yamazaki, H. & Kamykowski, D. The vertical trajectories of motile phytoplankton in a wind-mixed water column. *Deep-Sea Res.* **38,** 219–241 (1991).
18. Anis, A. & Moum, J. N. Surface wave-turbulence interactions: scaling $\epsilon(z)$ near the sea surface. *J. Phys. Oceanogr.* **25,** 2025–2045 (1995).
19. Prézelin, B. B., Boucher, N. P. & Smith, R. C. in *Ultraviolet Radiation in Antarctica: Measurements and Biological Effects* (eds Weiler, C. S. & Penhale, P. A.) 159–186 (Am. Geophys. Union, Washington DC, 1994).
20. Helbling, E. W., Villafañe, V., Ferrario, M. & Holm-Hansen, O. Impact of natural ultraviolet radiation on rates of photosynthesis and on specific marine phytoplankton species. *Mar. Ecol. Prog. Ser.* **80,** 89–100 (1992).
21. Zepp, R. G. & Cline, D. M. Rates of direct photolysis in aquatic environment. *Environ. Sci. Technol.* **11,** 359–366 (1977).
22. Murray, A. G. & Jackson, G. A. Viral dynamics II: a model of the interaction of ultraviolet light and mixing processes on virus survival in seawater. *Mar. Ecol. Prog. Ser.* **102,** 105–114 (1993).
23. Vincent, W. F. & Roy, S. Solar ultraviolet-B radiation and aquatic primary production: damage, protection and recovery. *Environ. Rev.* **1,** 1–12 (1993).
24. Morel, A. Available, usable, and stored radiant energy in relation to marine photosynthesis. *Deep-Sea Res.* **25,** 673–688 (1978).
25. Cullen, J. J. & Neale, P. J. in *The Effects of Ozone Depletion on Aquatic Ecosystems* (ed. Häder, D.-P.) 97–118 (Landes, Austin, 1997).
26. Gregg, W. W. & Carder, K. L. A simple spectral solar irradiance model for cloudless maritime atmospheres. *Limnol. Oceanogr.* **35,** 1657–1675 (1990).
27. Davis, R. F., Lazin, G., Bartlett, J., Ciotti, A. & Stabeno, P. Remote sensing of a pigment patch in the southeastern Bering Sea. *Proc. SPIE* **2963,** 654–657 (1997).
28. Prieur, L. & Sathyendranath, S. An optical classification of coastal and oceanic waters based on the specific absorption curves of phytoplankton pigments, dissolved organic matter, and other particulate materials. *Limnol. Oceanogr.* **26,** 671–689 (1981).
29. Sakshaug, E., Johnsen, G., Andersen, K. & Vernet, M. Modeling of light-dependent algal photosynthesis and growth: experiments with Barents Sea diatoms *Thalassiosira nordenskioeldii* and *Chaetoceros furcellatus*. *Deep-Sea Res.* **38,** 415–430 (1991).
30. Denman, K. L. & Gargett, A. E. Time and space scales of vertical mixing and advection of phytoplankton in the upper ocean. *Limnol. Oceanogr.* **28,** 801–815 (1983).

Acknowledgements. We thank members of the science team, officers and crew of the *Nathaniel B. Palmer* cruise NBP93-6 for assistance, W. Helbling, C. Gallegos, J. Christian, M. Lewis and B. Nieke for comments, D. Kelley for discussions of vertical mixing, M. Lesser for use of his spectroradiometers and P. Franks for providing his version of the mixing model. This work was supported by the NSF Office of Polar Programs, NSERC, NASA, and ONR Ocean Optics.

Correspondence and requests for materials should be addressed to J.J.C. (e-mail: John.Cullen@Dal.CA).

Increased polar stratospheric ozone losses and delayed eventual recovery owing to increasing greenhouse-gas concentrations

Drew T. Shindell, David Rind & Patrick Lonergan

NASA Goddard Institute for Space Studies and Center for Climate Systems Research, Columbia University, 2880 Broadway, New York, New York 10025, USA

The chemical reactions responsible for stratospheric ozone depletion are extremely sensitive to temperature[1]. Greenhouse gases warm the Earth's surface but cool the stratosphere radiatively[2–5] and therefore affect ozone depletion. Here we investigate the interplay between projected future emissions of greenhouse gases and levels of ozone-depleting halogen species using a global climate model that incorporates simplified ozone-depletion chemistry. Temperature and wind changes induced by the increasing greenhouse-gas concentrations alter planetary-wave propagation in our model, reducing the frequency of sudden stratospheric warmings in the Northern Hemisphere[4]. This results in a more stable Arctic polar vortex, with significantly colder temperatures in the lower stratosphere and concomitantly increased ozone depletion. Increased concentrations of greenhouse gases might therefore be at least partly responsible for the very large Arctic ozone losses observed in recent winters[6–9]. Arctic losses reach a maximum in the decade 2010 to 2019 in our model, roughly a decade after the maximum in stratospheric chlorine abundance. The mean losses are about the same as those over the Antarctic during the early 1990s, with geographically localized losses of up to two-thirds of the Arctic ozone column in the worst years. The severity and the duration of the Antarctic ozone hole are also predicted to increase because of greenhouse-gas-induced stratospheric cooling over the coming decades.

Parametrized chemistry was included interactively in the Goddard Institute for Space Studies (GISS) Global Climate/Middle Atmosphere Model (GCMAM)[10], a primitive equation model including parametrized gravity waves. This model has $8° \times 10°$ resolution (latitude × longitude), with 23 vertical layers extending from the surface to 85 km. Mountain wave drag was reduced globally to one-quarter its usual value[11] to allow realistic simulation of Southern Hemisphere polar lower-stratospheric temperatures, which were otherwise too warm. Modelled ozone transport was fixed at climatological values. This includes only zonal mean motions, so that we may underestimate the amount of chemical processing by longitudinally asymmetric motion of air across low-temperature regions. Ozone transport changes induced by increasing greenhouse gases were calculated non-interactively. We performed a control run without greenhouse gas forcing, and a run with forcings (Fig. 1), each including the chlorine loading trend[1,12,13]. Both began in 1959, allowing time for removal of any influence of initial conditions, and continued to the end of 2070. The atmosphere was coupled to a mixed-layer ocean with specified

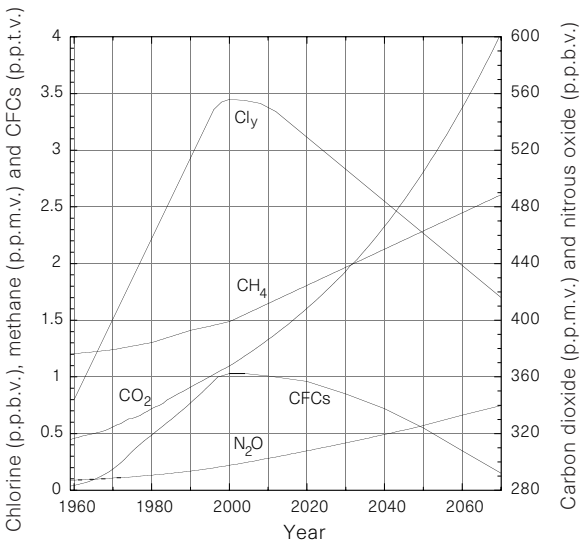

Figure 1 Emission trends for CO_2, N_2O, CH_4, CFCs and chlorine (Cl*y*) used as input to the model runs. Projected lower stratospheric chlorine loading (independent of height or latitude) is based on the trend derived from the 1992 Copenhagen revisions to the 1987 Montreal Protocol on Substances that Deplete the Ozone Layer[1], normalized slightly upwards and decreasing more slowly in the future to match recent observations[12,13,30]. Greenhouse-gas emissions are based on observations to the end of 1984, and subsequently are similar to, though for carbon dioxide slightly lower than, the 1992 International Panel on Climate Change (IPCC) preferred scenario IS92a[25]. The exception is CFCs, for which a steady reduction after 2000 has been assumed, consistent with their expected phase-out and with the chlorine loading scenario.